Hindawi
Mathematical Problems in Engineering
Volume 2022, Article ID 3917775, 12 pages
https://doi.org/10.1155/2022/3917775

Research Article

Low Voltage Ride through Enhancement Using Grey Wolf Optimizer to Reduce Overshoot Current in the Grid-Connected PV System

N. Jaalam, A.Z. Ahmad, A. M. A. Khalid, R. Abdullah, N. M. Saad, S. A. Ghani, and L. N. Muhammad

Faculty of Electrical & Electronics Engineering, University of Malaysia Pahang, 26600 Pekan, Malaysia

Correspondence should be addressed to N. Jaalam; zila@ump.edu.my

Received 5 November 2021; Revised 17 March 2022; Accepted 30 March 2022; Published 6 May 2022

Academic Editor: Amin Jajarmi

In today's world, the DG should not be disconnected in the event of a power outage but should instead remain linked to the grid and supported by reactive power. This can be accomplished by implementing the low voltage ride through (LVRT) with a proportional integral (PI) controller. As a result, the voltage profile can be enhanced. The PI controller, on the other hand, has drawbacks in that setting the gain takes a long time and results in an overshoot current on the grid, which could trigger the protection relay. To address this issue, this paper proposes employing a grey-wolf optimizer (GWO) to enhance the LVRT in a 5 MW three-phase grid-connected PV system. A MATLAB simulation was carried out then under a three-phase fault and load disturbance to verify the efficiency. It is found that, even with a 70% voltage sag, the PV system can remain connected to the electrical grid while minimising overshoot current on the grid side.

1. Introduction

The grid-connected PV system often experiences balance and unbalance voltage sags that are caused by short circuits and the connection of large loads. According to IEEE 1547, if a voltage sag occurs at the point of common coupling (PCC) during a grid fault, the grid must be disconnected immediately to preserve the power converters, and the inverter should not actively participate in voltage/var regulation, especially at low levels of PV penetration. However, with the high penetration of solar PV generators into the grid, stability issues may arise on the grid side if there is a disconnection of the PV plant during the fault. Furthermore, if the disconnection is repeated, the component lifetime will be negatively impacted, and the reconnection of the PV plant to the utility grid will necessitate substantial start-up costs [1]. Therefore, the inverter should stay connected to the grid within a permissible time and inject some reactive power to support the grid during voltage sags [1, 2]. This new requirement which is known as a LVRT, is an important practise in grid-connected PV systems nowadays to prevent long-term voltage instability that may lead to power outages [3]. Malaysia's LVRT limitation curve is depicted in Figure 1. If the voltage decrement value for the particular time range is above the red line, the distributed generation (DG) should stay connected to the grid while maintaining normal operation. However, if the voltage decrement value is less than the red line, the DG can be disconnected right away to avoid more serious damage, and this is the exact time for the anti-islanding to happen.

LVRT can be divided into 2 categories: either by adding external devices such as energy storage systems or supercapacitors [4], flexible alternating current transmission system (FACTS) devices [5], and braking chopper, or by modifying the internal inverter controller as shown in Figure 2. The latter method is getting massive attention now as it does not require any external device, so it will be cheaper and simpler. It is based on a control algorithm that can be

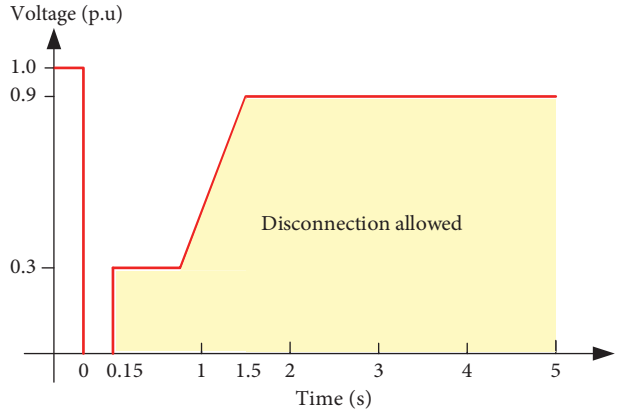

Figure 1: The LVRT limiting curve of Malaysia.

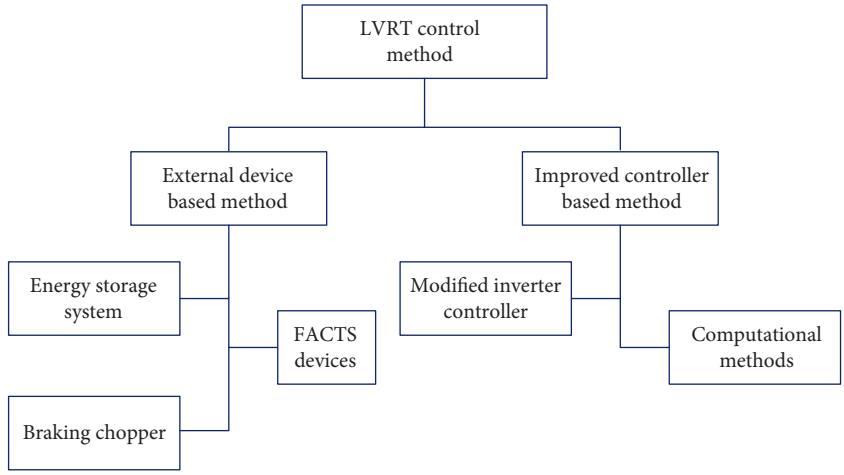

Figure 2: LVRT control method.

utilised using proportional integral (PI), proportional-resonant (PR), droop control, fuzzy logic controller, and particle swarm optimization (PSO) [6–10].

In the previous study, the inverter controller was successfully modified internally to provide reactive power into the grid during weak grid conditions using a PI controller [3, 11]. The PI controller has wide application in the industry due to its simplicity and effectiveness and does not need a more sophisticated approach [12]. However, in the power system industry, the rise of renewable energy penetration into the grid has brought uncertainty about the effectiveness of the PI controller [13]. The use of the PI controller will lead to an overshoot current on the grid side that can have a negative impact on the stability and operation of the power system. The PI controller tuning process also takes a long time because of the trial-and-error method used and does not produce good performance when it operates in a wide range of conditions [13, 14].

Thus, a metaheuristic algorithm that has already been well-known over the last two decades has now gained more interest in enhancing the LVRT strategy. It is a popular choice for obtaining accurate parameters as it is a simple, flexible, robust, and derivation-free mechanism [15]. Authors in [5] use neural networks (NNs) to detect grid faults in a grid-connected PV system. When a voltage sag is detected, a finite control set model predictive control (FCS-MPC) will provide reactive power support to enhance the LVRT capability. A probabilistic wavelet fuzzy neural network (PWFNN) and a Takagi–Sugeno–Kang probabilistic fuzzy neural network (TSKPFNN) were presented in [16, 17] to accommodate the LVRT requirement for power balance during various grid fault situations. It consists of a 6-layer feedforward neural network which consists of an input layer, membership layer, probabilistic layer, TSK-type fuzzy interference mechanism layer, rule layer, and output layer, all of which require an online learning algorithm. Both simulation and experimental results of this research have confirmed that this approach is able to stabilise the voltage under grid disturbance. However, the drawback of this approach lies in the complexity of the controller in confronting the uncertainties of the PV system. Meanwhile, a study on neurofuzzy controllers has been presented in [18] to enhance the LVRT. It is found that the proposed controller is effective in providing the required reactive power, but the output current at the PCC side is not present. Thus, it is not clear whether the overshoot current is present or not.

In this study, the PI controller will be tuned by GWO (GWO-PI) to compute the value of the proportional and

integral gain. The GWO algorithm was chosen as it is simple and can be easily programmed with speedy convergence [19]. The main objectives of the study are first to provide the required reactive power during the fault disturbance and second, to reduce the overshoot current in the grid-connected photovoltaic system. Based on Tenaga Nasional Berhad (TNB) distribution system parameters, a simulation model of a 5 MW PV system which is connected to a 33 kV grid will be developed using MATLAB/Simulink, as shown in Figure 3. A balanced three-phase fault with a load disturbance will be applied to see how well the proposed method works.

2. Methodology

This section will present the strategies applied to achieve the objectives of the study which can be divided into two parts: PV modelling and controller design.

2.1. PV Modelling. A single diode model, as shown in Figure 4, is used for PV modelling due to its simplicity and accuracy for power system analysis [18]. For more accurate results, series resistance R_s and shunt resistance R_{sh} can be added. However, the R_{sh} value is normally very large. Therefore, it is always neglected to reduce complexity.

By applying Kirchhoff's law, the mathematical equation for this model is given by (1) where I_{ph} represents the photocurrent, I_D is a diode current, and I_{PV} is the output current of the PV cell. The parameters of the system used in this study are listed in Table 1 which is based on the Suntech Power STP270-24/V_b solar PV module.

$$I_{\text{pv}} = I_{\text{ph}} - I_D. \tag{1}$$

From Table 1, one single Suntech Power STP270-24/Vb module can only generate 270 W. Hence, the PV module needs to be connected in parallel and series configurations to increase its current and voltage, respectively. When PV cells are joined in series, the voltage increases, whereas when PV cells are connected in parallel, the current increases. 28 series modules with 665 parallel strings are used to create a 5 MW PV system, as shown in the following calculation:

28 series module x $I_{\text{mp}} = 215.88$ A

665 parallel strings x $V_{\text{mp}} = 665 \times 35 = 23275$ V

215.88 A × 23275 V = 5.02 MW

2.2. Controller Design. The LVRT requirement specifies that when the voltage sag happens, the PV-DG should stay connected to the grid for a certain period of time, and at the same time, reactive current injection (RPI) should be provided to improve the voltage profile. For the successful implementation of the LVRT in faulty-mode operation, two major steps must be considered: the fault detection method and RPI. A fast and accurate fault detection method is crucial as it will determine the efficiency of the proposed LVRT system. In a weak grid condition, the system must be able to switch from normal operation to faulty-mode operation immediately for the LVRT with the RPI controller to take place. Figure 5 shows a flow chart of the system where the

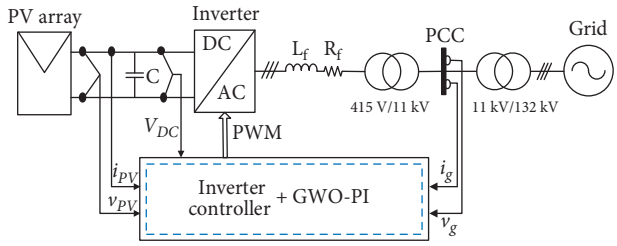

Figure 3: Basic structure of grid-connected PV system.

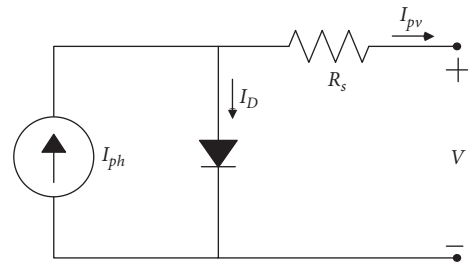

Figure 4: A simplified PV equivalent circuit with R_s only.

Table 1: PV model parameters.

Parameters	Values
Nominal peak power, P_m (W)	270
Nominal current, I_{mp} (A)	7.71
Nominal voltage, V_{mp} (V)	35
Short circuit current, I_{sC} (A)	8.2
Short circuit voltage, V_{sC} (A)	44.5
Series resistor, R_s (Ω)	0.32
Coefficient, K_i (%/K)	0.06
Total number of cells in series, N_s	72
Total number of cell in parallel, N_p	1

grid voltage, v_g will be continuously monitored to check whether it is still in the permissible range or not. If v_g is less than the normal grid voltage, $v_{gn,}$ two conditions must be checked, whether it is in the permissible range for more than 0.6 s or not. If so, the inverter must be disconnected from the grid immediately. Otherwise, the reactive power must be injected using GWO-PI to improve and stabilise the voltage profile. So, the PV inverter does not have to be disconnected from the grid to keep working.

To regulate the reactive power, a conventional method employing a PI controller can be used as shown in Figure 6 where the reactive current reference i_q^* is given by (2). However, it is very time consuming to determine the right value for the proportional gain (K_p) and integral gain (K_i). In addition, it always takes a long time to restore to its steady-state value after any fault clearance due to the error accumulation in the integral part of the PI controller, and sometimes overshoot current may occur [20].

$$i_q^* = K_p e + K_i \int e(t)\mathrm{d}t. \tag{2}$$

Therefore, to overcome this problem, a GWO-PI technique that imitates the leadership hierarchy and hunting mechanism of grey wolves is proposed. It is a meta-heuristic

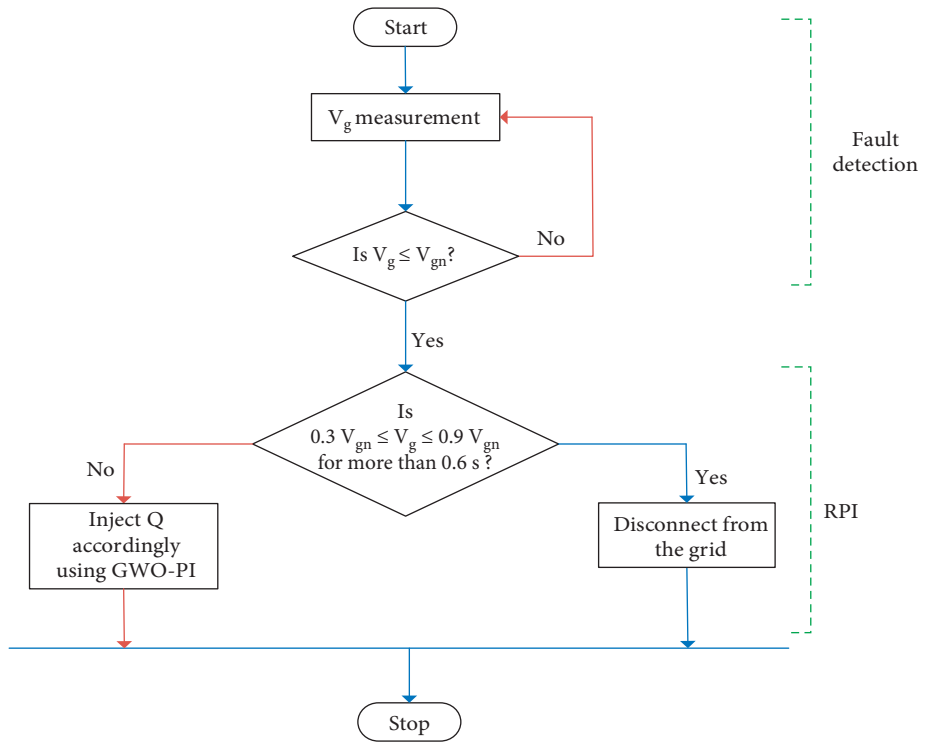

Figure 5: Flow chart of the proposed LVRT using GWO-PI.

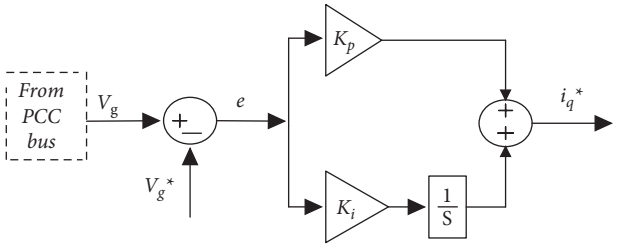

Figure 6: PI-based controller block diagram.

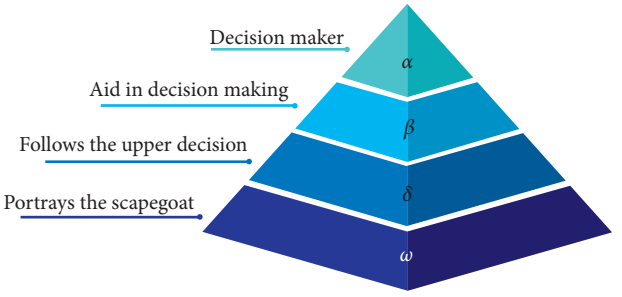

Figure 7: Social hierarchy of grey wolves.

algorithm that was introduced by Muro et al. and Mirjalili et al. [15, 21]. The grey wolf is an apex predator that is at the top of the food chain. Usually, five to twelve grey wolves would live together in a group. Figure 7 depicts the social hierarchy of the grey wolves. Alpha is the leader who makes the decisions about hunting, sleeping space, and other matters. Alpha is supported by beta to aid in decision making. Alpha will be replaced by beta if alpha is ill or dead. Omega is the lowest-ranking character, and he plays the role of a scapegoat. Delta follows the decisions of alpha and beta but is more dominant than omega. In the GWO algorithm, alpha is the fittest solution, beta is the second-best solution, while delta is the third best solution. Figure 8 shows the hunting behaviour of the grey wolves, and the three main stages of wolf hunting are as follows:

(i) Tracking, chasing, and approaching the prey

(ii) Pursuing, encircling, and harassing the prey until it stops moving

(iii) Attack towards the prey

For the fitness function, the integral time absolute error (ITAE) as in (3) is used to gain the controller parameters. In the MATLAB editor, the GWO code is executed while considering the fitness function, number of iterations, number of variables, and particles. Meanwhile, the ITAE value that was calculated in Simulink will be sent to the workspace where the GWO is employed. The optimised PI parameters are obtained after the GWO algorithm completes its iteration which will determine the character of the system. Figure 9 shows the GWO-PI controller feedback control system while Figure 10 depicts the flow chart of the algorithm.

$$\text{ITAE} = ft|\epsilon|\mathrm{d}t. \tag{3}$$

To provide reactive current $i^*_{q\text{new}}$ to the grid, the algorithm shown in (4) is used. The reference grid voltage v_g^* will be first compared with the measured grid voltage v_g. The error difference e produced by v_g and v_g^* will be utilised by the GWO to compute the proportional gain (Kp) and integral

Figure 8: Hunting behaviour of grey wolves: (a) Chasing, approaching, and tracking prey. (b–d) Pursuing, harassing, and encircling. (e) Stationary situation and attack [21].

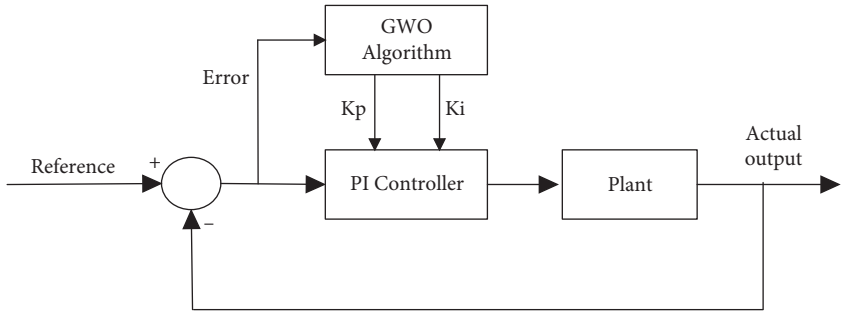

Figure 9: GWO-PI controller block diagram.

gain (Ki) with the maximum reactive current i^*_{qmax} defined by equation (5). The upper boundary is set to 40 and 5000 for the Kp and Ki while both lower boundaries are set to 0.

$$i^*_{q\,\text{new}} = \begin{bmatrix} 0, & \text{case } a\text{: } v_g > 0.9v_{gn}, \\ 2 - 2\dfrac{V_g}{V_{gn}}, & \text{case } b\text{: } 0.9v_{gn} \geq v_g \geq 0.3v_{gn}, \\ 1, & \text{case } c\text{: } v_g \leq 0.3v_{gn}, \end{bmatrix}, \tag{4}$$

$$i^*_{q\,\max} = \sqrt{i_n^2 - i_d^{*\,2}}. \tag{5}$$

The mathematical modelling of the GWO can be outlined as follows:

(i) Social hierarchy: for GWO, alpha (α) is considered the fittest solution, followed by beta (β) and delta (δ) as the second and third best solutions, respectively.

(ii) Encircling the prey: the encircling of prey can be expressed in the following equations:

$$\begin{aligned} \vec{D} &= \vec{C} \cdot \vec{X}(t) - \vec{X}(t), \\ \vec{X}(t+1) &= \vec{X}(t) - \vec{A} \cdot \vec{D}, \end{aligned} \tag{6}$$

(i) where $\vec{A}$ and $\vec{C}$ represent coefficient vectors, t is the current iteration, $\vec{X}$ is the position vector of the grey wolf, and $(X \cdot \vec{P})$ is the position vector of the prey. Meanwhile, $\vec{A}$ and $\vec{C}$ are vectors that can be calculated by using the following equations:

$$\begin{aligned} \vec{A} &= 2\vec{a} \cdot \vec{r}_1 - \vec{a}, \\ \vec{C} &= 2 \cdot \vec{r}. \end{aligned} \tag{7}$$

(iii) Hunting: the hunting is led by α, β, and δ ability to detect prey and encircle them. The other

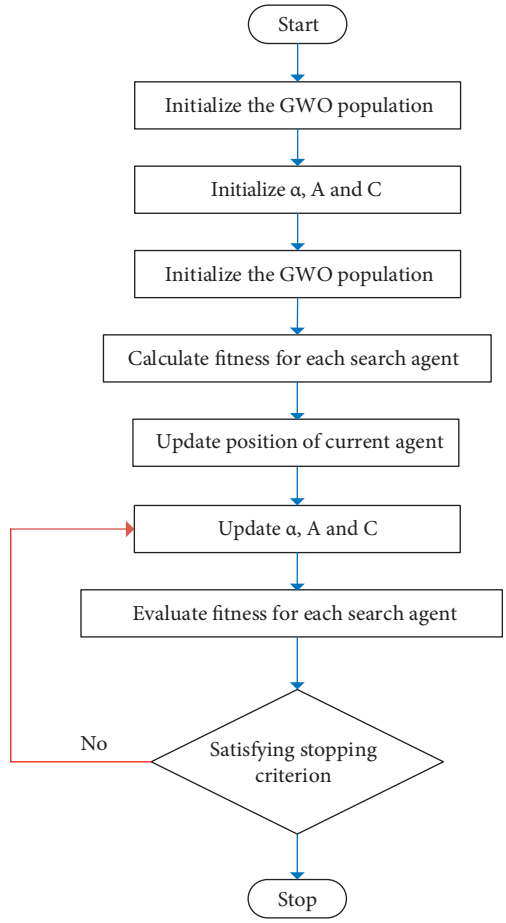

Figure 10: Flow chart of GWO.

search agents will update their positions according to the position of the best search agent. The following equations express this behaviour:

$$\vec{D}_{a\{3,8} = \vec{C}_{1,3}\vec{X}_{a\{3,8} - \vec{X},$$

$$\vec{X}_{1,3} = \vec{X}_{a,\{3,8} - \vec{A}_{1,3}\vec{D}_{a,\{3.8},$$

$$\vec{X}(t+1) = \frac{\vec{X}_1 + \vec{X} + \vec{X}_3}{3}. \quad (8)$$

(iv) Attacking the prey: the grey wolves will attack the prey when there are halts in the movement of the prey. For every iteration, α decreased from 2 to 0.

(v) Searching for prey: the exploration of the GWO algorithm is formulated based on the positions of α, β, and δ wolves. The wolves diverge during the search for prey and then converge to attack the prey.

3. Results

Two case studies were performed using MATLAB Simulink to validate the effectiveness of the proposed control strategy: one with a 20% voltage drop and the other with a 30% voltage drop, both with a balanced three-phase fault and load disturbances. With a 0.5 MW load connected, the fault occurred between 3.5 and 3.65 s in both situations. During 4.5 s to 5 s, another 0.1 MW load is applied.

3.1. 20% Voltage Drop. For the 20% voltage drop case, the number of iterations is 30, with the number of search agents set to 5. The convergence curve for this simulation is shown in Figure 11, with the best optimal value of the objective function obtained by the GWO being 0.014546. When the optimization is completed, the best solution gained by GWO is 40 and 3188.5158, which is the optimised value for K_p and K_i. Figure 12 shows the voltage profile comparison between systems with GWO-PI, PI only, and without RPI (NO RPI). Under normal conditions, the reactive current, $i_q = 0$, because there is no reactive power being injected, as shown in Figure 13. Therefore, the voltage dropped to 189.82 V when the fault happened at 3.5 s which accounted for more than 20% of the nominal value. The voltage dropped further when the load was connected at 4.5 s. With PI and GWO-PI based controllers, the voltage has successfully increased to 239.6 V as both controllers were able to inject the desired reactive power and have completely reduced the voltage drop to zero, thus grid disconnection can be avoided. However, the PI controller has a high overshoot voltage, but the GWO-PI

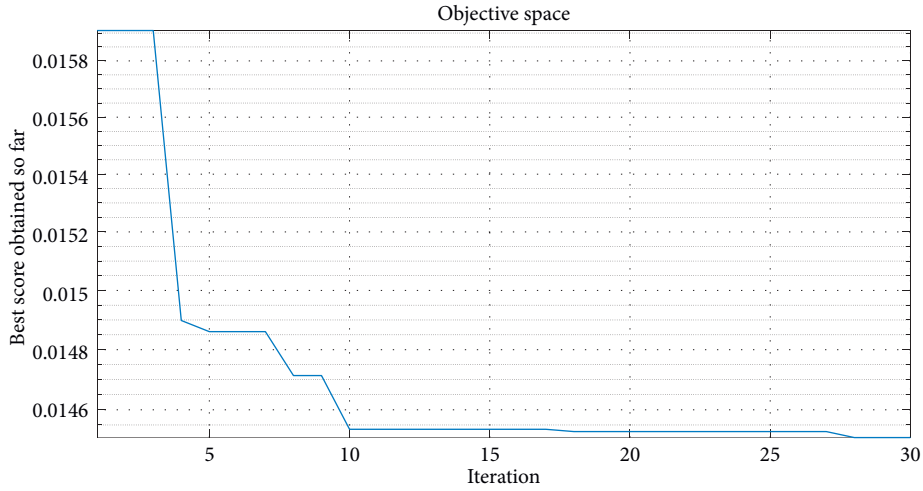

Figure 11: Convergence curve at 20% voltage drop.

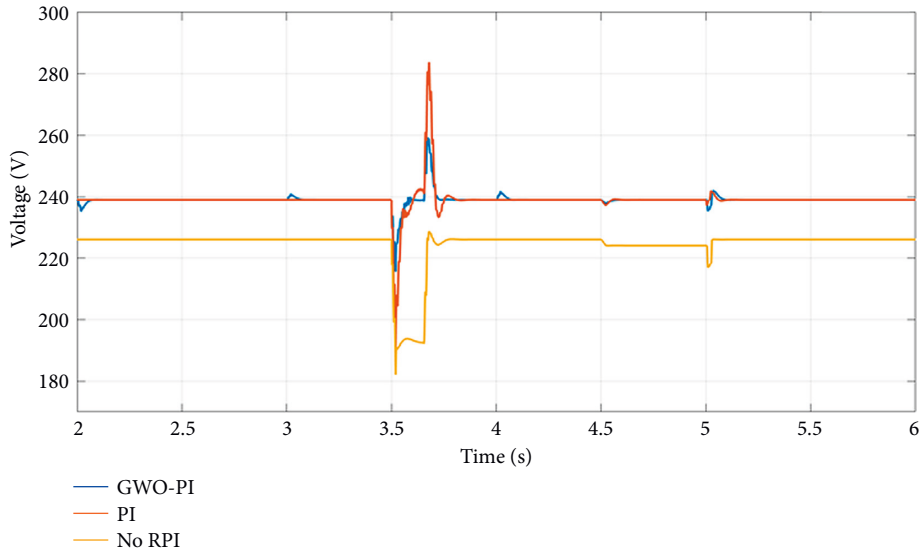

Figure 12: Voltage profile comparison at 20% voltage drop.

manages to reduce it by 8%. Meanwhile, Figure 14 shows the active and reactive power of the GWO-PI controller. When the fault occurs at 3.5 s, the reactive power increases significantly while the active power tries to maintain its power generation since the voltage drop is not severe. Table 2 summarises the performance of all controllers.

3.2. 30% Voltage Drop. For the second case, the number of iterations set is also 30. The number of search agents is 5. Figure 15 shows the convergence curve for this case where the best optimal value of the objective function found by GWO is 0.014509. After the optimization stopped, the best solution obtained by GWO was 40 and 4076.8579 which is the optimised value for K_p and K_i. Figure 16 illustrates the voltage profile comparison between GWO-PI, PI, and NO RPI. Without the RPI controller, the voltage drops by 30% to 168 V. With the PI and GWO-PI controllers, the reactive power can be injected accordingly as shown in Figure 17. Therefore, the voltage profile was improved as the voltage drop decrement has been reduced by at least 15%. The voltage significantly increased to 203.73 V for the PI and 238.03 V for the GWO-PI. Using GWO-PI, not only the highest value of reactive power can be injected, but it also shows the fastest settling time compared to the PI controller, as summarised in Table 3. During the fault condition, the

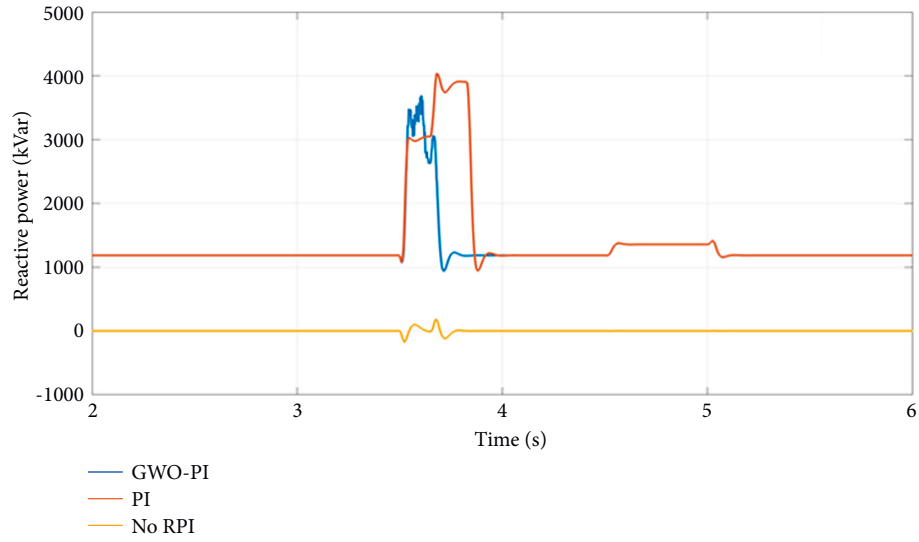

Figure 13: Reactive power comparison at 20% voltage drop.

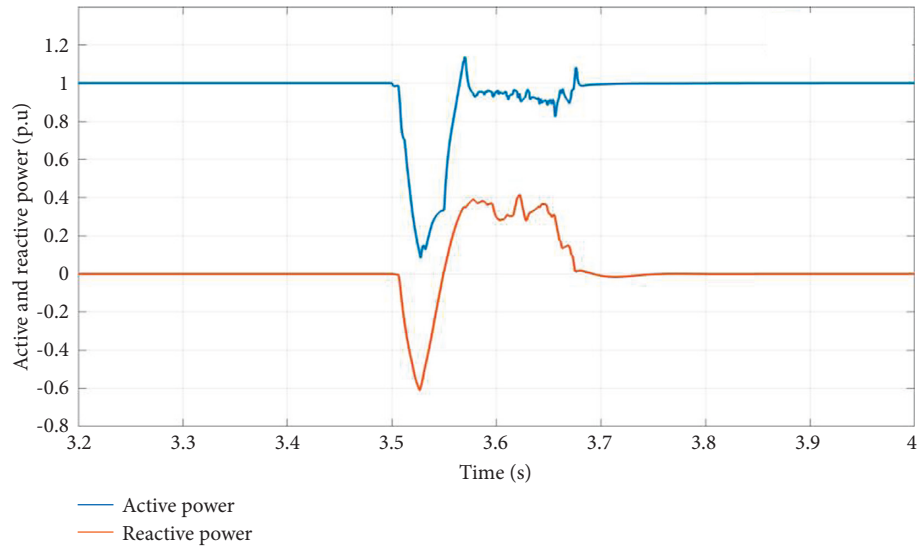

Figure 14: Active and reactive power for the GWO-PI controller.

Table 2: Controller performance comparison at 20% voltage drop.

	NO RPI	PI	GWO-PI
Voltage during fault (V)	189.82	239	239
Percentage of voltage drop (%)	20.91	0	0
Reactive power (kVar)	0	3763.54	3421.52
Overshoot voltage (%)	-	17.92	7.5

supply of active power should be limited to give sufficient room for the inverter to provide maximum reactive power as shown in Figure 18. Meanwhile, Figure 19 shows the grid or PCC current and voltage (phase A) under a 30% voltage drop with the PI controller. It can be seen that the current and voltage are not in phase when the fault occurs, and a high overshoot current is also noticeable. However, the GWO-PI controller was able to reduce this overshoot by

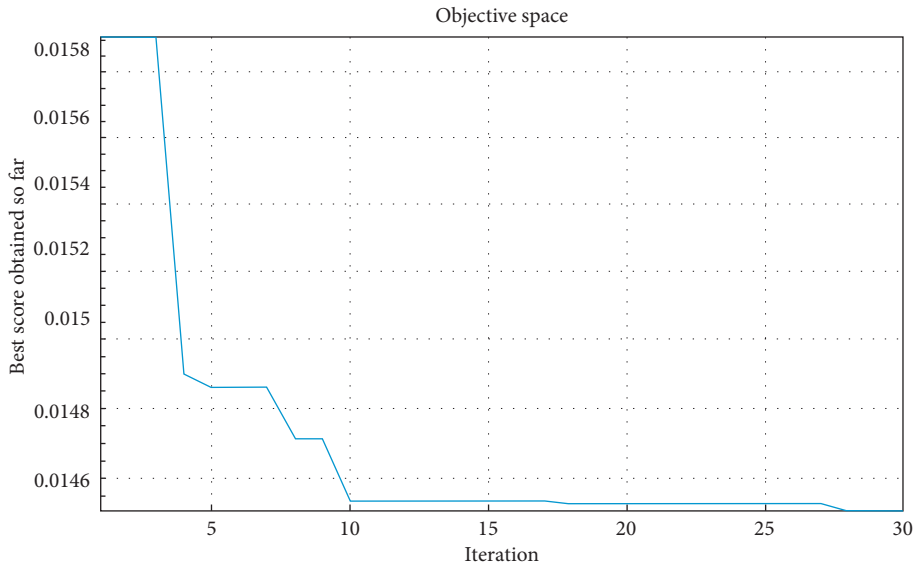

Figure 15: Convergence curve of the GWO.

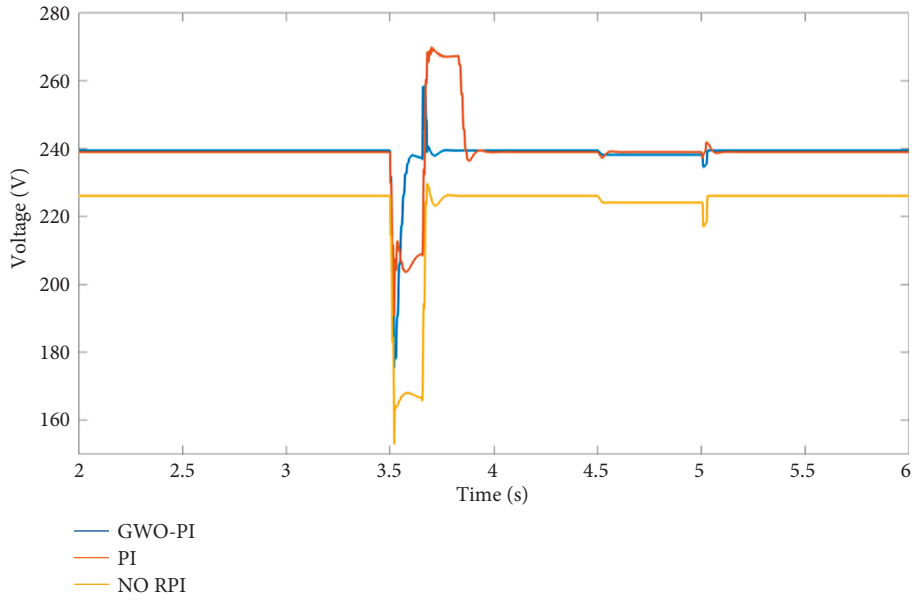

Figure 16: Voltage profile comparison at 30% voltage drop.

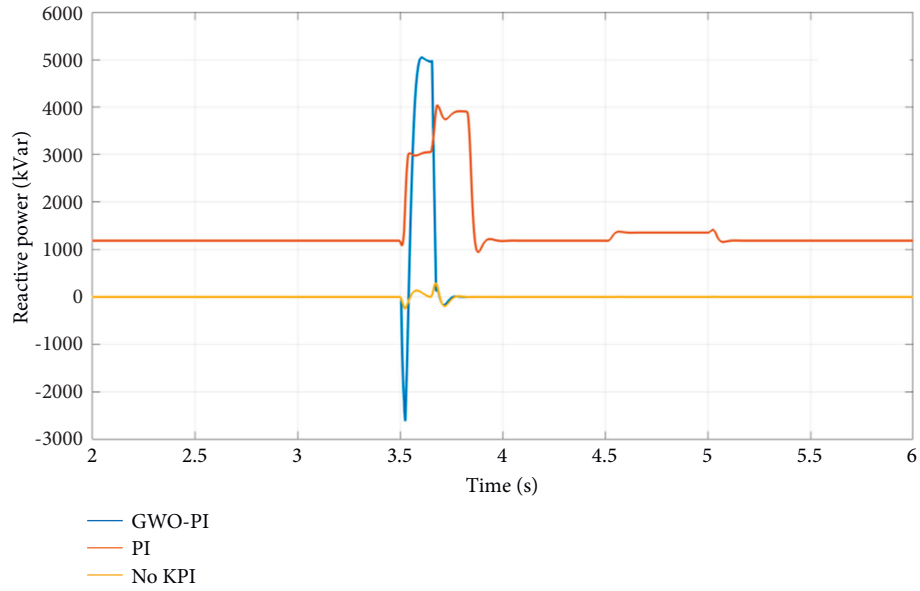

Figure 17: Reactive power comparison at 30% voltage drop.

Table 3: Controller performance comparison at 30% voltage drop.

	NO RPI	PI	GWO-PI
Voltage during fault (V)	168.01	203.73	238.03
Percentage of voltage drop (%)	30	15.4	0.83
Reactive power (kVar)	0	3763.18	4987.61
Voltage settling time (s)	-	0.29	0.13
Overshoot current	-	4.8	0.5

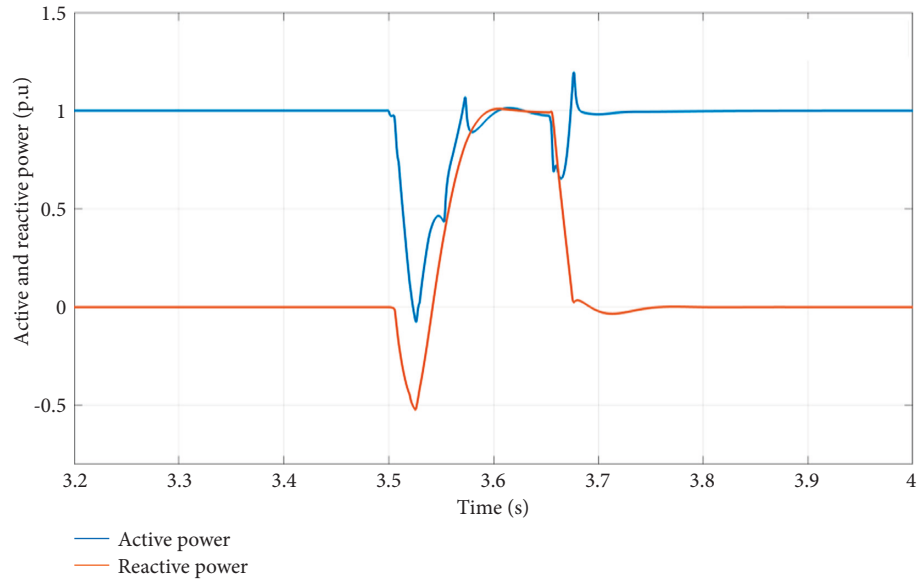

Figure 18: Active and reactive power of the GWO-PI controller.

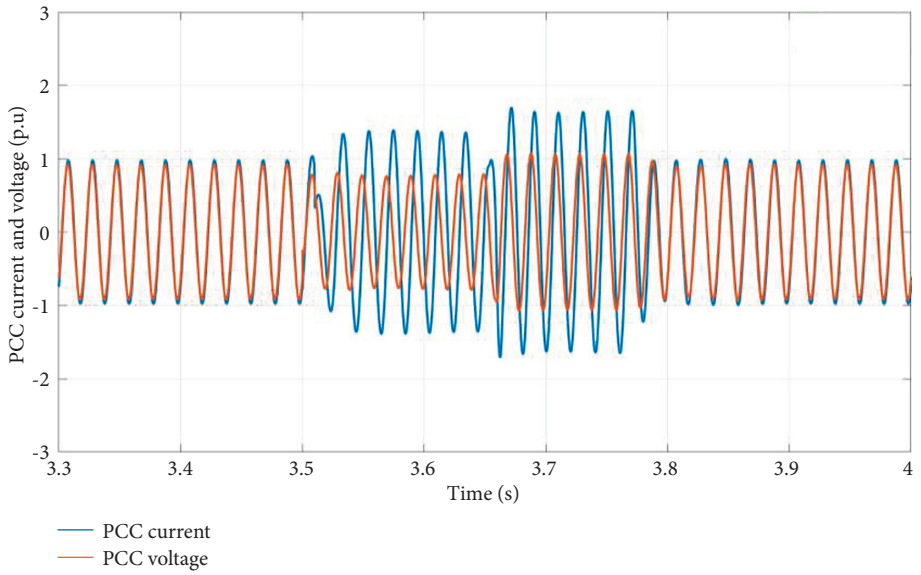

Figure 19: PCC current and voltage with PI controller.

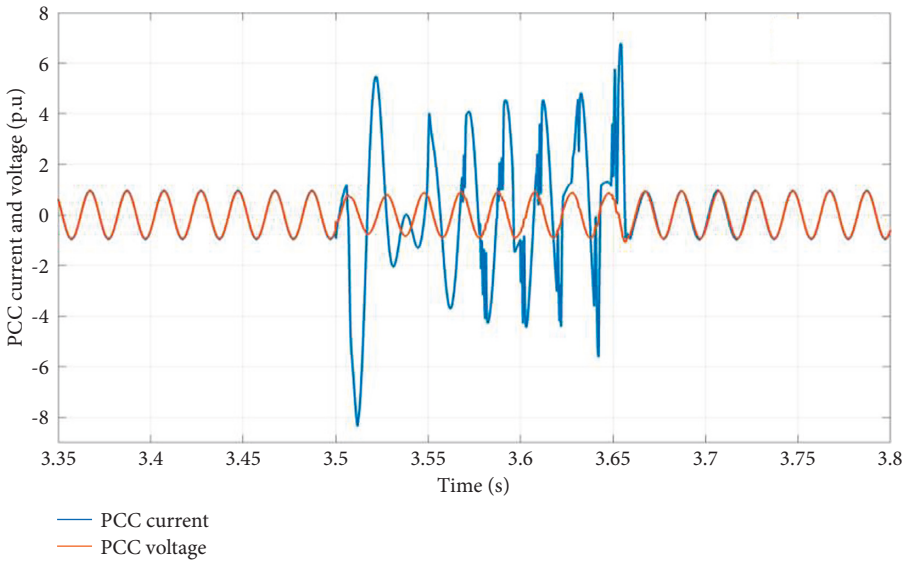

Figure 20: PCC current and voltage with GWO-PI controller.

approximately 4%, as illustrated in Figure 20. Table 3 summarises the performance of all controllers under 30% voltage sag.

4. Conclusion

This paper presents a new control strategy for the LVRT enhancement of the three-phase grid-connected PV system using the GWO-PI controller. The MATLAB simulation is used to assess the system's performance under a balanced three-phase fault and load disturbance. In a nutshell, it is found that the GWO-PI approach is more efficient than the PI controller. Even though both controllers are effective in compensating the desired reactive power during weak conditions, especially under 70% voltage sag, the GWO-PI controller managed to minimise the overshoot current. Besides, it can also significantly reduce the time it takes to tune the PI parameters. Even so, the proposed controller needs to be tested in more severe weak grid situations in the future including those caused by asymmetrical faults.

Data Availability

The GWO coding used to support the findings of this study are available from the corresponding author upon request.

Conflicts of Interest

The authors declare that they have no conflicts of interest.

Acknowledgments

The authors would like to thank the Ministry of Higher Education and the University of Malaysia Pahang for providing financial support under an internal research grant (Grant Number: RDU200329).

References

[1] N. Gira and A. K. Dahiya, "Solar PV-BES in distribution system with novel technique for DC voltage regulation," *Engineering Science and Technology, an International Journal*, vol. 23, no. 5, pp. 1058–1067, 2020.

[2] N. Hamrouni, S. Younsi, and M. Jraidi, "A flexible active and reactive power control strategy of a LV grid connected PV system," *Energy Procedia*, vol. 162, pp. 325–338, 2019.

[3] N. Jaalam, N. A. Rahim, A. H. A. Bakar, and B. M. Eid, "Strategy to enhance the low-voltage ride-through in photovoltaic system during multi-mode transition," *Solar Energy*, vol. 153, pp. 744–754, 2017.

[4] I. Hamdan, A. Maghraby, and O. Noureldeen, "Stability improvement and control of grid-connected photovoltaic system during faults using supercapacitor," *SN Applied Sciences*, vol. 1, no. 12, pp. 1–19, 2019.

[5] M. A. Khan, A. Haque, V. S. B. Kurukuru, and S. Mekhilef, "Advanced control strategy with voltage sag classification for single-phase grid-connected photovoltaic system," *IEEE Journal of Emerging and Selected Topics in Industrial Electronics*, vol. 3, no. 2, pp. 258–269, 2022.

[6] M. Mirhosseini, J. Pou, and V. G. Agelidis, "Single-stage inverter-based grid-connected photovoltaic power plant with ride-through capability over different types of grid faults," *IECON 2013 - 39th Annual Conference of the IEEE Industrial Electronics Society*, vol. 1, pp. 8008–8013, 2013.

[7] M. Mirhosseini, J. Pou, and V. G. Agelidis, "Single- and two-stage inverter-based grid-connected photovoltaic power plants with ride-through capability under grid faults," *IEEE Transactions on Sustainable Energy*, vol. 6, no. 3, pp. 1150–1159, 2015.

[8] F. Yang, L. Yang, and X. Ma, "An advanced control strategy of PV system for low-voltage ride-through capability enhancement," *Solar Energy*, vol. 109, pp. 24–35, 2014.

[9] M. M. Hasaneen, M. A. L. Badr, and A. M. Atallah, "Control of active/reactive power and low-voltage ride through for 40 kW three-phase grid-connected single-stage PV system," *CIRED - Open Access Proceedings Journal*, vol. 2017, no. 1, pp. 1655–1659, 2017.

[10] O. Noureldeen, I. Hamdan, and B. Hassanin, "Design of advanced artificial intelligence protection technique based on low voltage ride-through grid code for large-scale wind farm generators: a case study in Egypt," *SN Applied Sciences*, vol. 1, no. 6, pp. 1–19, 2019.

[11] Y. Yang, H. Wang, and F. Blaabjerg, "Reactive power injection strategies for single-phase photovoltaic systems considering grid requirements," in *Proceedings of the 2014 IEEE Applied Power Electronics Conference and Exposition - APEC 2014*, pp. 371–378, Fort Worth, TX, USA, March 2014.

[12] F. Khavari, A. Badri, and A. Zangeneh, "Energy management in multi-microgrids considering point of common coupling constraint," *International Journal of Electrical Power & Energy Systems*, vol. 115, no. 2020, Article ID 105465, 2020.

[13] W. Liu, Y. Zheng, Q. Chen, and D. Geng, "An adaptive CGPC based anti-windup PI controller with stability constraints for the intermittent power penetrated system," *International Journal of Electrical Power & Energy Systems*, vol. 130, Article ID 106922, 2021.

[14] Z. Ahmad and S. N. Singh, "An improved single phase transformerless inverter topology for grid connected PV system with reduce leakage current and reactive power capability," *Solar Energy*, vol. 157, pp. 133–146, 2017.

[15] S. Mirjalili, S. M. Mirjalili, and A. Lewis, "Grey wolf optimizer," *Advances in Engineering Software*, vol. 69, pp. 46–61, 2014.

[16] F.-J. Lin, K.-C. Lu, and T.-H. Ke, "Probabilistic wavelet fuzzy neural network based reactive power control for grid-connected three-phase PV system during grid faults," *Renewable Energy*, vol. 92, pp. 437–449, 2016.

[17] F.-J. Lin, K.-C. Lu, T.-H. Ke, B.-H. Yang, and Y.-R. Chang, "Reactive power control of three-phase grid-connected PV system during grid faults using Takagi-Sugeno Kang probabilistic fuzzy neural network control," *IEEE Transactions on Industrial Electronics*, vol. 62, no. 9, pp. 5516–5528, 2015.

[18] N. Jaalam, A. M. A. Haidar, N. L. Ramli, N. L. Ismail, and A. S. M. Sulaiman, "A neuro-fuzzy approach for stator resistance estimation of induction motor," in *ProceeInECCE 2011 - International Conference on Electrical, Control and Computer Engineering*, pp. 394–398, Kuantan, Malaysia, June 2011.

[19] S. Padhy, S. Panda, and S. Mahapatra, "A modified GWO technique based cascade PI-PD controller for AGC of power systems in presence of plug in electric vehicles," *Engineering Science and Technology, an International Journal*, vol. 20, no. 2, pp. 427–442, 2017.

[20] N. H. Saad, A. A. El-Sattar, and A. E.-A. M. Mansour, "Improved particle swarm optimization for photovoltaic system connected to the grid with low voltage ride through capability," *Renewable Energy*, vol. 85, pp. 181–194, 2016.

[21] C. Muro, R. Escobedo, L. Spector, and R. P. Coppinger, "Wolf-pack (*Canis lupus*) hunting strategies emerge from simple rules in computational simulations," *Behavioural Processes*, vol. 88, no. 3, pp. 192–197, 2011.